Title: Thresholds for post-rebound SHIV control after CCR5 gene-edited autologous hematopoietic cell transplantation

Authors: E. Fabian Cardozo-Ojeda[1], Elizabeth R. Duke[1,4], Christopher W. Peterson[2,3,4], Daniel B. Reeves[1], Bryan T. Mayer[1], Hans-Peter Kiem[2,3,4,5], Joshua T. Schiffer[1,2,4,*]

Affiliations:

[1]Vaccine and Infectious Disease Division,

[2]Clinical Research Division,

[3]Stem Cell and Gene Therapy Program, Fred Hutchinson Cancer Research Center, Seattle, WA, USA;

[4]Department of Medicine and

[5]Department of Pathology, University of Washington, Seattle, WA, USA.

* To whom correspondence should be addressed. Address: 1100 Fairview Ave. N. MS E4-100, Seattle, WA, 98119; email: jschiffe@fredhutch.org; phone: (206)667-7359.

One Sentence Summary: Autologous transplantation of ΔCCR5 HSPCs may induce post-ATI SHIV control when the gene-edited cell dose is sufficient to overcome SHIV immunity loss.

Abstract: Autologous, CCR5 gene-edited hematopoietic stem and progenitor cell (HSPC) transplantation is a promising strategy for achieving HIV remission. However, only a fraction of HSPCs can be edited *ex vivo* to provide protection against infection prior to autologous transplantation. The optimal transplantation conditions for achieving viral control in the absence of suppressive antiretroviral therapy (ART) are still unknown. We analyzed data from SHIV-1157ipd3N4-infected juvenile pig-tailed macaques that underwent autologous HSPC transplantation with and without CCR5 gene editing. We developed a mathematical model that recapitulates reconstitution of T cell subset counts and SHIV plasma viral loads in control and transplanted macaques. The model predicts that viral control can be obtained following ART treatment interruption (ATI) when: 1) levels of transplanted HSPCs are at least 10-fold higher than residual endogenous HSPCs after total body irradiation and 2) the fraction of protected HSPCs in the transplant achieves a threshold (73%-90%) sufficient to overcome transplantation-dependent loss of SHIV immunity. Under these conditions, if ATI is withheld until transplanted gene-modified cells engraft and reconstitute to a steady state, then spontaneous viral control is projected to occur immediately. Our results support strategies that 1) increase stem cell dose, 2) enhance potency of conditioning regimen, 3) elevate fraction of gene modified SHIV-resistant cells, 4) extend periods between HSPC transplantation and ATI with tracking of $CD4^{+}CCR5^{-}$ cell recovery and / or 5) augment anti-SHIV immunity to achieve sustained SHIV remission.

[Main Text:]

Introduction

The major obstacle to HIV-1 eradication is a latent reservoir of long-lived, infected cells (*1-3*). Cure strategies aim to eliminate all infected cells or permanently prevent viral reactivation from latency. The only known case of HIV cure (*4, 5*) and an additional recently-reported case of prolonged remission (*6*) resulted from allogeneic hematopoietic stem cell transplant with homozygous CCR5Δ32 donor cells (*4-6*). The success of this procedure is likely multifactorial—in part attributable to HIV resistance of the transplanted cells, the conditioning regimen that facilitates engraftment and eliminates infected cells, graft-versus-host effect against residual infected cells, and immunosuppressive therapies for graft-versus-host disease (*7-10*).

We are interested in recapitulating this method of cure with minimal toxicity. Specifically, we are investigating the use of autologous transplantation following *ex vivo* inactivation of the CCR5 gene with gene-editing (*11, 12*). This procedure is safe and feasible in pigtail macaques infected with simian-human immunodeficiency virus (SHIV) (*12-14*) and is currently being investigated in a Phase I clinical trial in suppressed, HIV-1-infected individuals (NCT02500849). Also, this approach is more broadly applicable because an allogeneic CCR5-negative donor is not needed. However, current data suggests that protocols do not achieve sufficient fractions of genetically modified HIV-resistant HSPCs. In contrast, in allogeneic transplant nearly 100% of circulating immune cells after engraftment consist of donor-derived CCR5Δ32 cells. This leads to a key question: what threshold percentage of CCR5-edited, autologous HSPCs is necessary for the cure/long term remission observed in the Berlin and London patients?

To answer this question, we developed a mathematical model that predicts the minimum threshold of gene-modified cells necessary for functional cure. First, we modeled the kinetics of $CD4^+CCR5^+$, $CD4^+$ $CCR5^-$, and $CD8^+$ T cell reconstitution after autologous transplantation.

Then we modeled SHIV kinetics during acute infection and rebound following ART treatment interruption to identify the degree of loss of anti-HIV cytolytic immunity following transplantation. Finally, we applied our models to predict the proportion of gene-modified cells necessary for stable virus remission, the dose of these cells relative to the intensity of the preparative conditioning regimen (total body irradiation, TBI), the timing of subsequent ATI, and the levels of SHIV-specific immunity required to maintain virus remission following ATI. Results from this three-part modeling approach support strategies that 1) increase stem cell dose, 2) enhance potency of conditioning regimen, 3) elevate fraction of gene modified SHIV-resistant cells, 4), extend periods between HSPC transplantation and ATI with tracking of CCR5- cell recovery and / or 5) augment anti-HIV immunity to achieve sustained HIV remission.

Results

Study design and mathematical modeling

We analyzed data from 22 juvenile pig-tailed macaques that were intravenously challenged with 9500 TCID50 SHIV1157ipd3N4 (SHIV-C) (**Fig. 1A**). After 6 months of infection, the macaques received combination ART that included tenofovir (PMPA), emtricitabine (FTC), and raltegravir (RAL). When on ART, 17/22 received total body irradiation (TBI) followed by the transplantation of autologous HSPCs with (n=12) or without (n=5) CCR5 gene editing (ΔCCR5 and WT groups, respectively). A control group (n=5) did not receive TBI or HSPC transplantation. 14 of the animals underwent ATI approximately one year after ART initiation. The remaining 8 animals were necropsied at an earlier time relative to the other animals' ATI (see Methods for details).

To analyze the data and estimate thresholds for viral control under this approach we used ordinary differential equation models. We performed multi-stage modeling (**Fig. 1B**). First, we modeled the kinetics of $CD4^+$ and $CD8^+$ T cell subsets after autologous HSPC infusion following transplant and before ATI, assuming that ART suppression decouples SHIV- from cellular-dynamics. After validation of the first-stage model, we introduced a second-stage modeling to 1) explain virus and T cell kinetics during primary infection and analytical treatment interruption (ATI) and to 2) identify the degree of loss of anti-HIV cytolytic immunity due to the preparative conditioning. Then, we used the final validated model to project SHIV kinetics assuming different transplantation conditions.

$CD4^+CCR5^+$ and $CD8^+$ T cells recover more rapidly than $CD4^+CCR5^-$ T cells after HSPC transplantation.

We analyzed the kinetics of peripheral blood $CD4^+CCR5^+$ and $CD4^+CCR5^-$ T cells, and total, $T_{naïve}$, T_{CM}, and T_{EM} $CD8^+$ T cells in macaques after HSPC transplantation.

In untransplanted controls, levels of $CD4^+$ and $CD8^+$ T cells oscillated around a persistent set point (blue data-points in **Fig. 2**). Also, $CD4^+$ $CCR5^+$ T cell levels were ~100 cells/μL and were uniformly lower than the $CD4^+CCR5^-$ T counts (each ~1000 cells/μL) (**Fig. S1A**). Finally, total $CD8^+$ T cell levels in the control group were ~1400 cells/μl with a greater contribution from T_{EM} (73%) than T_N+T_{CM} (27%) (based on median values, **Fig. S1B**).

In the transplant groups, post-TBI levels of $CD4^+CCR5^+$, $CD4^+CCR5^-$ and $CD8^+$ T cells were significantly lower than in the control group but expanded at different rates during the following weeks (**Fig. 2A-C**). The levels of $CD4^+CCR5^+$ T cells started at 1-10 cells/μl and reconstituted to levels similar to the control group over 5-10 weeks (**Fig. 2A-B**). $CD4^+CCR5^-$ T

cells remained at higher levels (~100 cells/μL) than $CD4^+CCR5^+$ T cells after TBI but expanded more slowly and did not reach the values of the control group after 25 weeks (**Figs. 2A-B**). The $CD4^+CCR5^+$ T cell compartment expanded 8-fold more rapidly than the $CD4^+CCR5^-$ compartment (p=0.01, paired t-test, **Figs. 2C**). $CD8^+$ T cells decreased to levels between 10 and 100 cells/μl after TBI but recovered to levels below the control group in 5 weeks (**Figs. 2A-B**); $CD8^+$ T cells recovered as rapidly as the $CD4^+CCR5^+$ population (**Figs. 2C**).

Overall, these results show that after transplantation $CD4^+CCR5^+$ and $CD8^+$ T cells recover faster than $CD4^+CCR5^-$ cells. This suggest that each cell subset may have different and/or complementary mechanisms that drive their expansion. To explore these mechanisms, we analyzed the data with a mechanistic mathematical model of cellular dynamics.

Lymphopenia-induced proliferation drives early $CD4^+CCR5^+$ and $CD8^+$ T cell reconstitution after HSPC transplantation.

To identify the main drivers of T cell reconstitution after transplant, we developed a mathematical model that considered plausible mechanisms underlying reconstitution of distinct T cell subsets following autologous transplantation (**Fig. 3A**). We assumed that T cell reconstitution may have two main drivers: (1) lymphopenia-induced proliferation of mature cells that persists through myeloablative TBI (*15-19*), and (2) differentiation from naïve cells from progenitors in the thymus (from transplanted $CD34^+$ HSPCs (*20, 21*) or residual endogenous $CD34^+$ HSPCs that persist following TBI) and further differentiation to an activated effector state (*19, 22-26*). We also assumed the infused product dose D contains a fraction f_p of transplanted, gene-edited HSPCs that do not express CCR5 (See **Table S1** for individual values of D and f_p). Thus, in our model ΔCCR5-gene-modified $CD4^+$ T cells differentiating from these

modified HSPCs are subset of the total $CD4^+CCR5^-$ cell compartment (**Fig. 3A**), and therefore they have the same reconstitution kinetics.

We built 12 versions of the model by assuming that one or multiple mechanisms are absent, or by assuming certain mechanisms have equivalent or differing kinetics (**Table S2**). Using model selection theory, we identified the most parsimonious model that reproduced the data (schematic in **Fig. 3A** without red-dashed lines). The best model predictions for each cell subset using maximum likelihood estimates of the population parameters (**Table S3**) are presented in **Fig. 3B**. Individual fits are visualized in **Figs. S2-S4** and parameter estimates are collected in **Table S4**.

Model selection illuminated several biological phenomena: 1) $CD4^+CCR5^+$ T cell reconstitution after transplant is determined by cell proliferation and to a minor degree by upregulation of CCR5 (**Fig. 3C**); 2) $CD4^+CCR5^-$ T cell expansion is driven primarily by new naïve cells from the thymus and to a lesser extent by CCR5 downregulation (**Fig. 3C**); and 3) thymic export is not significantly different for $CD4^+$ or $CD8^+$ T cells (**Table S2**).

This first-stage modeling also makes testable biological predictions. First, the estimated $CD4^+CCR5^+$ T cell proliferation rate (~0.1/day) far exceeds the estimated CCR5 upregulation (~0.004/day) and thymic export rates (~0.002/day). Therefore, one month after transplantation, the total concentration of $CD4^+CCR5^+$ T new cells generated by proliferation is predicted to be 40-fold higher than the concentration generated by up-regulation of CCR5 (**Fig. 3C**). Second, the $CD8^+$ T_{EM} cells comprise the majority of the total $CD8^+$ T cell compartment (**Fig. 3B**) with a proliferation rate up to 10-fold higher than the $CD8^+$ T_{CM} cell differentiation rate (**Fig. S5**). In this way, $CD8^+$ T cells follow a similar pattern to $CD4^+CCR5^+$ T cells (**Fig. 3B**).

In summary, following autologous HSPC transplant: 1) thymic export and downregulation of CCR5 drive a modest expansion of $CD4^+CCR5^-$ T cells, whereas 2) rapid lymphopenia-induced proliferation after TBI is the main driver for $CD4^+CCR5^+$ and $CD8^+$ T cell expansion, which are derived from both the transplanted HSPC product and residual endogenous cells that persisted through the myeloablative conditioning regimen.

Reduced $CD4^+CCR5^+$ T cell counts correlate with post-ATI plasma viral rebound only in animals that underwent HSPC transplantation without CCR5 editing.

We compared plasma viral load rebound kinetics (*13*, *27*) to $CD4^+CCR5^+$ and $CCR5^-$ T cell subset dynamics after ART treatment interruption (ATI). **Fig. 4** presents the plasma viral loads and the blood $CD4^+CCR5^+$ and $CD4^+CCR5^-$ T cell kinetics before and after ATI in transplanted and control macaques. Viral burden after ATI was higher in the wild-type (WT) transplant group compared to the control and ΔCCR5 groups. Median peak viral load was 10-fold higher (p=0.06 comparing WT and control groups, Mann-Whitney test. **Fig. 4A**). Median viral load measurements at time of necropsy were 2-$\log_{10}$ higher (p=0.06 comparing WT and control groups, Mann-Whitney test. See **Fig.4B**). $CD4^+CCR5^+$ T cell counts decreased after ATI in the WT group, reaching a significantly lower nadir (~8-fold) than in the control animals (p=0.01 comparing WT and control groups, Mann-Whitney test. **Fig. 4C**). The two animals with the largest reduction of $CD4^+CCR5^+$ T cells had the highest viral set points in the WT group. A similar trend was not observed in the ΔCCR5 group. There was no difference between $CD4^+CCR5^-$ T cell nadirs in the control and transplant groups (**Fig. 4D**).

In the control and ΔCCR5 groups individual viral loads did not correlate with corresponding $CD4^+CCR5^+$ T cell counts post-ATI. However, in three out of the four animals in

the wild-type transplant group, viral load observations post-ATI correlated negatively with their corresponding $CD4^+CCR5^+$ T cell counts (**Fig. S6**). To summarize, only animals that were transplanted with wild-type HSPCs had higher viral loads that correlated with reductions in $CD4^+CCR5^+$ T cells and more rapid disease progression after ATI. When CCR5-editing was included in the transplanted HSPC product, viral rebound and the degree of T cell depletion was more similar to the control group (no transplantation). We hypothesize that transplantation augments depletion of $CD4^+CCR5^+$ T cells following ATI, which can be rescued via ΔCCR5 edition of the HSPC product.

A reduction in SHIV-specific immunity leads to higher viral rebound set points and $CD4^+CCR5^+$ T cell depletion following ATI in transplanted animals.

We simultaneously analyzed the viral and T cell subset data using mechanistic mathematical models in order to understand how transplantation modifies plasma viral load and $CD4^+CCR5^+$ T cell kinetics during ATI. We extended our T cell reconstitution model to include SHIV infection (**Fig. 5A** and **Methods**) and used this second-stage model to analyze virus and T cell dynamics from SHIV-infection until ATI. Again following model selection theory based on AIC, we found the most parsimonious model to explain the data (**Fig. 5A**, **Table S5**). This model simultaneously recapitulates plasma viral load and the kinetics of $CD4^+$ $CCR5^+$ and $CCR5^-$ T cells during primary infection and rebound after ATI in each animal as shown in **Fig. 5B** and **Figs. S7-S9** with corresponding estimated parameters in **Tables S6-S7**. In this model, SHIV-specific $CD8^+$ effector cells reduce virus production rather than killing infected cells (*28-30*), possibly by secretion of HIV-antiviral factors (*31-33*)—not explicitly included in the model. The model also suggests that infection enhances upregulation of $CD4^+CCR5^-$ T cells. This

upregulation replenishes $CD4^+CCR5^+$ T cells and transiently reduces the $CD4^+CCR5^-$ compartment after ATI (*34-36*). Finally, the data-fit required different SHIV-specific $CD8^+$ T cell proliferation, saturation and death rates, i.e. parameters ω_8, I_{50} and d_h from **eq. 3**, respectively between ATI and acute infection (see **Table S5**) (*27*).

We used our model to calculate an approximate viral load set point (**Fig. 5C** and **Methods**) after treatment interruption. This set point is driven by the ratio between the turnover rate of SHIV-specific $CD8^+$ T cells and the virus production rate: $\frac{\left(\frac{\omega_8 K_m}{d_h}\right)}{\pi}$ (see **Methods**). This ratio correlates negatively with the measured final viral load (**Fig. 5D**). In this sense, the highest viral set point in animals in the transplant groups might be due to the underlying low immune response to the virus. However, we found that no individual SHIV-specific immunity parameter was correlated with viral set point or was different among the three groups. Rather, the only estimated parameter that differed among groups was the time until successful SHIV reactivation (t_{sa}, see **Methods**) which was significantly higher in the transplant groups (**Fig. 5E**). In conclusion, we developed a second-stage model that simultaneously recapitulates viral and T cell dynamics from SHIV-infected animals receiving autologous HSPC transplantation. This model implies that transplant reduces host T-cell immunity, resulting in higher viral loads after ATI in transplanted animals.

Post-ATI viral control requires a large HSPC dose containing a high fraction of CCR5-edited cells

An important advantage of our model is the ability to calculate the conditions required for post-ATI viral control (viral load set point < 30 copies/ml) after CCR5-edited autologous

transplant. To this end, we used our second-stage model to approximate an effective reproductive ratio R_{eff} to describe the ability of the virus to sustain infection after ATI (see **Methods**):

$$R_{eff} = R_T \left(1 - \frac{f_p D}{D + P_r}\right). \qquad \textbf{Equation (1)}$$

Here, f_p describes the fraction of protected HSPCs in the transplant product, D the dose or total number of infused HSPCs, and P_r the number of residual endogenous HSPCs after conditioning (variable P, **Fig. 3A**). R_T is the approximate number of new infections caused by one infected cell after T cell complete reconstitution post-conditioning as defined in **eq. 4** (see Methods) and is inversely related to the anti-SHIV immune response at the time of ATI. Post-ATI viral control depends on the number of HSPCs in the body immediately after transplant that are protected from SHIV infection, or $\left(\frac{f_p D}{D + P_r}\right)$.

To estimate the values of f_p, D, and P_r needed for viral control, we first estimated R_T for each animal based on individual parameter estimates pertaining to anti-SHIV immunity. We then simulated the model for each animal using varying values of f_p from zero to one (0-100% CCR5-edited HSPCs), values of D from 10^6 to 10^9 HSPCs, and values of P_r from zero to 10^7 HSPCs. As an illustration, **Fig. 6A** depicts projections of the model for transplanted animal A11219 for selected values of f_p when $D = 10^7$ HSPCs/kg and $P_r = 6 \times 10^6$ HSPCs. When f_p, D and P_r made $R_{eff} \geq 1$, plasma viremia rebounded following ATI and virus was not controlled. When $R_{eff} < 1$, post-rebound control was observed, but only at weeks 40-60 post-ATI, following an initial decrease in viral loads beginning 30-40 weeks after ATI. In this case, post-rebound control occurred concomitantly with ΔCCR5 $CD4^+$ T cell complete reconstitution relative to non-edited $CCR5^{+/-}$ $CD4^+$ T cells (**Fig 6B**). Lower values of R_{eff} resulted in earlier post-rebound control.

For all animals, post-treatment control occurred when values of f_p, D and P_r made $R_{eff} < 1$ (**Fig. S10**). Model predictions of animal A11200 demonstrate that regardless of the fraction of protected HSPCs in the transplant (f_p), viral control is possible only when the ratio of HSPCs in the transplant to the residual endogenous HSPCs in the body post-TBI ($D{:}P_r$) is above 10 (**Fig. 6C**). Moreover, if the ratio $D{:}P_r$ is greater than 10, the minimum fraction of protected cells required is 73%. When the ratio $D{:}P_r$ is higher than 100, we found that the minimum fraction of protected cells in the transplant f_p varied from 73% to 90% in all transplanted animals and was positively correlated with a weaker anti-SHIV immune response of the given animal defined by R_T (**Fig. 6D**). Similar results were obtained for all other animals (**Fig. S11**). This is consistent with **eq. 1** as $R_{eff} \approx R_T(1 - f_p)$ when $D \gg P_r$. R_T varied from 3 and 6 across animals using individual parameter estimates in **Table S7**. The required levels for f_p are lower in the context of more intense anti-SHIV immunologic pressure. This result argues for strategies that 1) sustain anti-SHIV immunity (lower R_T), 2) increase the stem cell dose relative to the residual endogenous stem cells ($D{:}P_r$) after transplant—perhaps by enhancing potency of the conditioning regimen, and 3) increase the fraction of gene-modified, SHIV-resistant cells (f_p).

Based on the observation the viral control occurred when $CD4^+$ T cell subsets reached a steady state in the simulations (**Fig. 6A-B)**, we simulated the model again for animal A11219 under conditions that lead to viral control: $f_p = 0.95$, $D = 10^{8.5}$ HSPCs and $P_r = 10^7$ HSPCs with ATI occurring at 3, 14, 26 or 38 weeks after transplantation. Indeed, time to post-ATI viral control (shaded areas in **Fig. 7A**) decreased as time to ATI was extended after transplant and as the difference between $CD4^+CCR5^-$ cell density at ATI and its expected set point decreased (shaded areas in **Fig. 7B**). In this case, $\Delta CCR5\, CD4^+$ T cells comprised the majority of the $CD4^+CCR5^-$ T cell compartment (**Fig. 7B**). When including varying times of ATI from 0 to 60

weeks after transplantation, the model predicted the time between transplant and ATI required to avoid viral rebound is about 30 weeks for animal A11219 (**Fig. 7C**). This timeframe allowed a $CD4^+CCR5^-$ cell density at ATI exceeding 80% of the ultimate steady state value (**Fig. 7D**).

In summary, our model predicts that post-ATI viral control during autologous HSPC transplantation is obtained when 1) the transplanted HSPC dose is significantly higher than the residual endogenous HSPCs that persist through myeloablative conditioning (in this case TBI) *and* 2) the fraction of protected (i.e. CCR5-edited) HSPCs in the transplant (f_p) is sufficiently high to outcompete cells susceptible to infection and disrupt ongoing cycles of viral replication. Spontaneous post-treatment control occurs after $CCR5^-$ $CD4^+$ T cells achieve a steady state approximately one-year after transplantation. Hence, our model suggests that prolonging time to ATI (at least one year post-transplantation). Moreover, specifically tracking $CD4^+CCR5^-$ T cell growth and waiting for steady-state could be used as a surrogate for the decision to undergo ATI.

Discussion

Here we introduce a data-validated mathematical model that, to our knowledge, is the first to simultaneously recapitulate viral loads as well as $CD4^+$ and $CD8^+$ T cell subset counts in a macaque model of suppressed HIV-1 infection. We systematically compared 12 models to arrive at a set of equations that most parsimoniously explains the available data. In multiple stages of modeling, we recapitulated (1) peripheral $CD4^+$ and $CD8^+$ T-cell subset reconstitution dynamics following transplant and (2) T-cell subset dynamics and SHIV viral rebound following ATI. Before ATI, all animals had suppressed plasma viral loads below the limit of detection, allowing analysis of T cell reconstitution dynamics independent of virus-mediated pressure. At each step, we applied model selection theory to select the simplest set of mechanisms capable of

explaining the observed data (*37*). Our model predicts that post-rebound viral control might be possible during autologous gene-edited HSPC transplantation if therapy achieves (1) a sufficient fraction of gene-protected, autologous HSPCs, (2) a high dose of transplant product relative to a residual endogenous population of stem cells that persists following conditioning, and (3) enhancement of SHIV-specific immune responses following transplantation.

Although the model predicts a potential benefit for more potent conditioning that favors engraftment of SHIV-resistant cells, a more myeloablative conditioning regimen may also deplete SHIV-specific immune responses and lead to less favorable toxicity profiles. We previously demonstrated the link between disruption of the immune response during transplant and increased magnitude of viral rebound during treatment interruption (*13, 27*). Here we predict that the magnitude of the SHIV-specific immune response is correlated not only with viral load set point, but also with the reduction of $CD4^{+}CCR5^{+}$ T cells after ATI. $CD4^{+}CCR5^{+}$ T cell depletion might also be reflective of the loss of depletion of virus-specific immunity following conditioning. In this case, a higher threshold of CCR5-gene-edited cells in the transplanted HSPC product would be required to obtain stable, ART-free viral control. These results are consistent with the cure achieved by the Berlin patient who received a transplant with 100% HIV-resistant cells after intense conditioning (*4, 5*). In the autologous setting where 100% CCR5 editing may not be feasible, adjunctive measures that augment virus-specific immunity, such as therapeutic vaccination, infusion of HIV-specific chimeric antigen receptor (CAR) T cells or use of neutralizing antibodies, may synergize with HSPC transplantation to achieve post-treatment control (*38, 39*).

Our results are somewhat limited by a small sample size of 22 animals. For that reason, several model parameters were assumed to be the same among the population (i.e., without

random effects). However, the number of observations for each animal was large enough to discriminate among several different plausible model candidates. Therefore, we performed projections using only the individual estimated parameters. Reassuringly, our results align with prior mechanistic studies of cellular reconstitution after stem cell transplantation (*15, 20, 40-42*). Our analysis also suggests that the majority of reconstituting $CD4^+CCR5^-$ T cells do not proliferate and have slow rates consistent with estimates of thymic export from previous studies (*20, 41, 42*).

Recent studies from our group and others make clear that although a preparative conditioning regimen (e.g. TBI) is essential to maximize engraftment of transplanted HSPCs, it does not clear 100% of host lymphocytes, especially those in tissues (*13, 14, 43, 44*). The best fitting model predicts that incomplete elimination of lymphocytes by TBI prevents $CD4^+CCR5^-$ cells from predominating post-transplant: the rapid expansion of $CD4^+CCR5^+$ and $CD8^+$ T cells during the first few weeks after HSPC transplantation is most likely due to lymphopenia-induced proliferation of residual endogenous cells after TBI rather than thymic reconstitution. $CD4^+CCR5^-$ T cells arising from thymic export of both transplanted and remaining cells are overwhelmed by more rapidly populating $CD4^+CCR5^+$ T cells within weeks of transplantation. Going forward, we will need to identify anatomic sites and (namely viral reservoir tissues such as spleen and lymph nodes) and associated mechanisms that allow activated $CD4^+CCR5^+$ to survive conditioning.

A final important observation from our model is that $CD4^+$ T cell kinetics conducive to viral control may not be reached 30 weeks after transplant. Therefore, our model suggests that ATI should be delayed until $CD4^+CCR5^-$ T cells reconstitute to their natural steady state.

Optimized timing of ATI would ideally be based on reconstitution of all $CD4^+$ and $CD8^+$ T cell subsets ensuring approximately steady state levels before discontinuing ART.

In conclusion, our mathematical model recapitulates, to an unprecedented degree of accuracy, the complex interplay between reconstituting HIV-susceptible $CD4^+$ T cells, HIV-resistant $CD4^+$ T cells, infected cells, virus-specific immune cells, and replicating virus following autologous, CCR5-edited HSPC transplantation. Our results illustrate the capabilities of mathematical models to glean insight from preclinical animal models and highlight that modeling will be required to optimize strategies for HIV cure.

Methods

Study Design

We employed a multi-stage approach using ordinary differential equation models of cellular and viral dynamics to analyze data from SHIV-infected pig-tailed macaques that underwent autologous HSPC transplantation during ART and to find conditions for post-rebound control when gene-edited cells were included in the transplant product. First, we modeled T cell dynamics and reconstitution following transplant and before ATI, assuming that low viral loads during suppressive ART do not affect cell dynamics (**Fig. 1B**). In the second stage, we added viral load data during primary infection and after ATI and fit models to the T cell and viral dynamics simultaneously from data pre- and post-ATI (**Fig. 1C**). We then used the most parsimonious model, as determined by AIC, to perform simulated experiments for different transplant conditions, focusing on variables including fraction of protected cells, dose, depletion of HSPCs after conditioning, and time of ATI after transplant to find thresholds for viral control post-ATI.

Experimental Data

Twenty-two juvenile pigtail macaques were intravenously challenged with 9500 TCID50 SHIV-1157ipd3N4 (SHIV-C) (*13, 14*). After 6 months, the macaques received combination antiretroviral therapy (ART): tenofovir (PMPA), emtricitabine (FTC), and raltegravir (RAL). After ~30 weeks on ART, 17 animals received total body irradiation (TBI) followed by transplantation of autologous HSPCs. In 12/17 animals the transplant product included CCR5 gene-edited HSPCs (ΔCCR5 group); HSPC products in 5/17 animals were not edited (WT group). After an additional 25 weeks following transplant, when viral load was well suppressed, animals underwent ATI (*13*). A control group of five animals did not receive TBI or HSPC transplantation and underwent ATI after ~50 weeks of treatment. One and six of the animals in the WT and ΔCCR5 groups, respectively, were necropsied before ATI. One of the animals in the control group was necropsied before ATI (**Fig. 1A**). Plasma viral loads and absolute peripheral T-cell counts from $CD4^+CCR5^-$, $CD4^+CCR5^+$ and total $CD8^+$ and subsets (naïve, central memory [T_{CM}], and effector memory [T_{EM}]) were measured for the control and WT group as described previously (*13*). We analyzed peripheral T cell counts and plasma viral load from transplant until 43 weeks post-transplant (~25 weeks pre-ATI and ~20 weeks post-ATI).

Mathematical modeling of T cell reconstitution dynamics

We modeled the kinetics of $CD4^+$ and $CD8^+$ T cell subsets in blood including residual endogenous, transplanted cells that home to the BM, and progenitor cells in the BM/thymus both from transplant and residual endogenous. We included $CD8^+$ T cells in the model because $CD8^+$ and $CD4^+$ T cells may arise from new naïve cells from the thymus and compete with each other

for resources that impact clonal expansion and cell survival (*15, 45, 46*). We assumed that expansion of $CD4^+$ and $CD8^+$ T cells in the blood derives from: (1) export of naïve cells differentiated from a progenitor compartment in the BM/Thymus (*40, 47*) (either from transplanted (*20, 21*) or residual endogenous $CD34^+$ HSPCs) and further differentiation to an activated effector state (*19, 22-26, 48-50*), or (2) lymphopenia-induced division of mature, residual endogenous cells that persist through myeloablative TBI (*15-19*) as factors that drive T cell proliferation are more accessible (i.e., self-MHC molecules on antigen-presenting cells (*22, 23, 51*) and γ-chain cytokines such as IL-7 and IL-15 (*16-18, 52*)). However, as they grow, cells compete for access to these resources, limiting clonal expansion (*15*) such that logistic growth models are appropriate (*45*).

In our mathematical model, transplanted HSPCs T home to the bone-marrow at a rate k_e. We assumed a single cell compartment for T cell progenitors in the bone marrow (BM)/thymus represented by variable P. We assumed that P renew logistically with maximum rate r_p, differentiate into naïve $CD4^+$ and $CD8^+$ T cells at rates λ_f and λ_e, respectively, or are cleared at rate d_p (*53-55*). We assumed two $CD4^+$ T cell compartments: SHIV-non-susceptible, i.e. $CD4^+$ T cells that do not express CCR5 ($CD4^+CCR5^-$ T cells) N, and a SHIV-susceptible compartment, S ($CD4^+CCR5^+$ T cells). Only the N compartment includes $CD4^+$ naïve cells migrating from the thymus (*56-58*) at an input rate $\lambda_f P$ cells per day (*20, 59*). N cells grow with maximum rate r_n, upregulate CCR5 (*24*) at rate λ_n, and are cleared from the periphery at rate d_n. The S compartment does not have a thymic input but can grow with maximum division rate r_s, downregulate CCR5 (*24*) at a rate λ_s, and are cleared at rate d_s. We model $CD8^+$ T cell reconstitution assuming a compartment for naïve and central memory cells, M, and a compartment for the effector memory subset, E. We assumed that M cells have thymic input of

$\lambda_e P$ cells per day, grow logistically with maximum division rate r_m, differentiate to effector memory at rate λ_m, and are cleared at rate d_m. The E compartment grows with maximum division rate r_e and is cleared at rate d_e. We added variables T_p, P_p and N_p, representing CCR5 gene-modified- transplanted HSPCs, T cell progenitor cells in BM/thymus, and blood $CD4^+CCR5^-$ T cells, respectively. These compartments have the same structure as T, P and N, but with two differences. First, the value of T_p at transplantation is a fraction f_p of the total number of infused cells. Second, the N_p cell compartment do not upregulate CCR5. We model the competition of $CD4^+$ and $CD8^+$ T cells for resources that allow cell division using a logistic equation that depends on the difference between the total number of competing cells, i.e. $A=N_p+N+S+M+E$, and a carrying capacity K (*15*). Under these assumptions we constructed the following model form:

$$\begin{aligned}
\frac{dT_p}{dt} &= -k_e T_p \\
\frac{dP_p}{dt} &= k_e T_p + \hat{r}_p\left(1-\frac{A}{K_p}\right)P_p \\
\frac{dN_p}{dt} &= \lambda_f P_p + \hat{r}_n\left(1-\frac{A}{K_n}\right)N_p \\
\frac{dT}{dt} &= -k_e T \\
\frac{dP}{dt} &= k_e T + \hat{r}_p\left(1-\frac{A}{K_p}\right)P \\
\frac{dN}{dt} &= \lambda_f P + \hat{r}_n\left(1-\frac{A}{K_n}\right)N + \lambda_s S \\
\frac{dS}{dt} &= \hat{r}_s\left(1-\frac{A}{K_s}\right)S + \lambda_n N \\
\frac{dM}{dt} &= \lambda_e(P+P_p) + \hat{r}_m\left(1-\frac{A}{K_m}\right)M \\
\frac{dE}{dt} &= \lambda_m M + \hat{r}_e\left(1-\frac{A}{K_e}\right)E
\end{aligned} \quad , \qquad \textbf{Equation (2)}$$

where $\hat{r}_p = r_p - (\lambda_f + \lambda_e + d_p)$, $\hat{r}_n = r_n - (\lambda_n + d_n)$, $\hat{r}_s = r_s - (\lambda_s + d_s)$, $\hat{r}_m = r_m - (\lambda_m + d_m)$, $\hat{r}_e = r_e - d_e$, as well as $K_w = K\frac{\hat{r}_w}{r_w}$ for each model variable $w \in \{p, n, s, m, e\}$.

When simulating the model, we assumed t_0 as the time of transplantation. For the transplant groups the system is in a transient stage due to conditioning (TBI) at t_0, therefore initial values cannot be obtained from steady state equations. Transplantation is modeled as $T(t_0) = (1 - f_p)D$ and $T_p(t_0) = f_p D$. For the control group we used t_0 at a similar time relative to the transplant groups. Since the control group did not have any transplantation or TBI, we assumed $T(t_0) = T_p(t_0) = P_p(t_0) = N_p(t_0) = 0$. Other initial values were calculated assuming steady state: $P(t_0) = \frac{q_2 q_3 q_4 K_p}{(q_1+1)q_3 q_4 + q2(q_4+1)}$, $N(t_0) = \frac{q_1 q_3 q_4 K_p}{(q_1+1)q_3 q_4 + q2(q_4+1)}$, $S(t_0) = \frac{q_3 q_4 K_p}{(q_1+1)q_3 q_4 + q2(q_4+1)}$, $M(t_0) = \frac{q_2 q_4 K_p}{(q_1+1)q_3 q_4 + q2(q_4+1)}$ and $E(t_0) = \frac{q_2 K_p}{(q_1+1)q_3 q_4 + q2(q_4+1)}$. Here $q_1 = \frac{\hat{r}_s}{\lambda_n}\left(\frac{K_p}{K_s} - 1\right)$, $q_2 = \frac{\hat{r}_n}{\lambda_f}\left(q_1\left(\frac{K_p}{K_n} - 1\right) - \lambda_s\right)$, $q_3 = \frac{\hat{r}_m}{\lambda_e}\left(\frac{K_p}{K_m} - 1\right)$ and $q_4 = \frac{\hat{r}_e}{\lambda_m}\left(\frac{K_p}{K_e} - 1\right)$. A parsimonious, curated version of this model was selected from a series of models with varying mechanistic and statistical complexity (**Table S2).**

Mathematical modeling of SHIV infection and T cell response dynamics

We next adapted the curated T cell reconstitution model by combining several adaptations of the canonical model of viral dynamics (*27, 60-66*). Here, virus *V* infects only $CD4^+CCR5^+$ T cells (*67*) *S* at rate β. We modeled ART by reducing the infection rate to zero. A fraction τ of the infected cells produce virus, I_p, and the other fraction become unproductively infected, I_u (*27, 68, 69*). I_P cells arise only from activation of a persistent set of latently infected cells at rate $\xi\bar{L}$. We modeled ATI by assuming infection β is greater than zero after some delay following ART interruption. We approximate this delay as the sum of the time of ART to washout (~3 days) and the time of successful activation (t_{sa}) of a steady set of latently infected cells. For simplicity, we assumed that $\xi\bar{L} = \frac{1}{t_{sa}}$ and assumed that t_{sa} has lognormal distribution

among the animal population with high variance (*70-72*). All infected cells die at rate δ_I (*27*). I_P cells produce virus at a rate π per cell, that is cleared at rate γ. CD8$^+$ M cells proliferate in the presence of infection with maximum rate ω_8. A fraction f of these cells become SHIV-specific CD8$^+$ effector T cells, E_h, that are removed at a rate d_h (*64, 65, 73*). These effector cells may reduce virus production (π) or increase infected cell clearance (δ_I) by $1/(1+\theta E_h)$ or by $(1+\kappa E_h)$, respectively (*28-30, 63, 74*). We assumed that non-susceptible CD4$^+$ T cells may upregulate CCR5 and replenish the susceptible pool during infection (*35, 36, 75*) with rate ω_4. For cell growth the total number of competing cells is given by $A = N_p+N+S+I_p+I_u+M+E+E_h$. The model in **eq. 2** is modified to include:

$$\begin{aligned}
\frac{dN}{dt} &= \lambda_f P + \hat{r}_n\left(1-\frac{A}{K_n}\right)N + \lambda_s S - \omega_4 \frac{I_p+I_u}{1+\frac{I_p+I_u}{I_{50}}}N \\
\frac{dS}{dt} &= \hat{r}_s\left(1-\frac{A}{K_s}\right)S + \lambda_n N - \beta V S + \omega_4 \frac{I_p+I_u}{1+\frac{I_p+I_u}{I_{50}}}N \\
\frac{dI_p}{dt} &= \tau\beta V S - \delta_I(1+\kappa E_h)I_p + \xi\bar{L} \\
\frac{dI_u}{dt} &= (1-\tau)\beta V S - \delta_I(1+\kappa E_h)I_u \\
\frac{dV}{dt} &= \frac{1}{1+\theta E_h}\pi I_p - \gamma V \\
\frac{dM}{dt} &= \lambda_e(P+P_p) + \hat{r}_m\left(1-\frac{A}{K_m}\right)M + \omega_8(1-2f)\frac{I_p+I_u}{1+\frac{I_p+I_u}{I_{50}}}M \\
\frac{dE_h}{dt} &= \omega_8 f \frac{I_p+I_u}{1+\frac{I_p+I_u}{I_{50}}}M - d_h E_h .
\end{aligned} \qquad \textbf{Equation (3)}$$

When simulating this model, we assume $t_0 = 0$ as the moment of SHIV challenge, and t_x as the moment of transplantation after challenge. We modeled conditioning by: (1) adding a term $-k_T C$ in all blood cell compartments $C \in \{N_p, N, S, I_p, I_u, M, E, E_h\}$ and (2) the term $-k_H P$ for the HSPC compartment P. k_T and k_H are different than zero only during the two days before transplant ($t_x - 2 \leq t < t_x$). Transplantation is modeled as an input only when $t = t_x$ to cell compartments T and T_p with amounts $(1-f_p)D$ and $f_p D$, respectively. A parsimonious version

of this model was selected from a series of models with varying mechanistic and statistical complexity (**Table S2).**

Fitting procedure and model selection

To fit our models (**eqs. 2, 3**) to the transplant data, we used a nonlinear mixed-effects modeling approach (*76*) described in detail in the **Supplementary Materials**. Briefly, we obtained a maximum likelihood estimation of the population median (fixed effects) and standard deviation (random effects) for each model parameter using the Stochastic Approximation Expectation Maximization (SAEM) algorithm embedded in the Monolix software (www.lixoft.eu). For a subset of parameters, random effects were specified, and the standard deviation values were estimated. Measurement error variance was also estimated assuming an additive error model for the logged outcome variables.

We first fit instances of models with varying statistical and mechanistic complexity in **eq. 2** to blood T cell counts during transplant and before ATI (**Fig. 1B**) assuming that one or multiple mechanisms are absent, or that certain mechanisms have equal kinetics (**Table S2** includes all 12 competing models with the different statistical assumptions). We fixed the HSPC homing rate k_e=1/day (*77, 78*), and f_p and D as described in **Table S1**. Since at t_0 the system is in a transient stage due to conditioning (TBI) we estimated blood cell concentrations at t_0, but fixed the number of HSPCs that remained in the bone marrow/thymus $P(t_0)$ to 6×10^6 based on the estimated minimum number of infused HSPCs needed for engraftment in the same animal model (*44*). All other parameters were estimated were estimated as described in **Supp. Materials** and **Table S2**.

Next, we fit several instances of the model in **eq. 3** to pre- and post-ATI blood T cell counts and plasma viral loads (**Fig. 1B**) using the best model obtained for **eq. 2** (**Table S5** includes all 4 competing models and respective statistical assumptions). At the time of SHIV infection, values for the cell compartments were calculated from steady state equations with the same form as for the group without transplantation ("control") in the previous section. $V(0)$ was fixed to a small value below the limit of detection, and $I_p(0)$ and $I_u(0)$ were calculated as $\tau c V(0)/\pi$ and $(1-\tau)cV(0)/\pi$, respectively. We fixed the following parameters: $\gamma = 23$/day (*79*), $\delta_I = 1$/day (*80, 81*), $\tau = 0.05$ (*68*) and $f = 0.9$ (*63*). The value of k_h was constrained to obtain a value of the HSPCs after conditioning $P(t_x) = P_r = 6 \times 10^6$ (*44*). We fixed values of t_x, f_p and D as described in **Table S1.** All other parameters were estimated as described in **Supp. Materials** and **Table S5**.

To determine the best and most parsimonious model among the instances, we computed the log-likelihood (log *L*) and the Akaike Information Criteria (AIC=-2log *L*+2*m*, where *m* is the number of parameters estimated) (*37*). We assumed a model has similar support from the data if the difference between its AIC and the best model (lowest) AIC is less than two (*37*).

Effective reproductive ratio when $r_n = 0$ *and* $\kappa = 0$

We calculated an approximate effective reproductive ratio R_{eff} for our model (**eqs. 2, 3**) by computing the average number of offspring produced by one productively infected cell I_p at ATI assuming all cell compartments have reached steady state after transplantation during ART. This number is the product of the average lifespan of one I_p, the virus production rate by this latently infected cell, the lifespan of produced virions from this cell, the rate at which each virion infects the pool of susceptible cells at steady state, the fraction of these infections that become

productive and the reduction of virus production, cell infection and cell death by SHIV-specific immune cells at ATI. Using this approach we obtain that $R_{eff} = \frac{\tau\beta\bar{S}\pi}{\gamma\delta_I(1+\theta\bar{E}_h)}$, with $\bar{S} \approx \frac{\lambda_f\bar{P}}{\frac{\hat{d}_n\hat{r}_s}{\lambda_n}\left(\frac{K_p}{K_s}-1\right)-\lambda_s}$ and $\bar{E}_h \approx \frac{f\omega_8\lambda_e K_p}{ad_h\delta_I t_{sa}\hat{r}_m\left(\frac{K_p}{K_m}-1\right)}$ the steady state values of variables S (SHIV-susceptible cells) and E_h (SHIV-specific effector cells) during ART with $a \approx \frac{\lambda_e}{\hat{r}_m\left(\frac{K_p}{K_m}-1\right)} + \frac{\lambda_f\lambda_n}{\hat{d}_n\hat{r}_s\left(\frac{K_p}{K_s}-1\right)-\lambda_s\lambda_n} + \frac{\lambda_f\hat{r}_s\left(\frac{K_p}{K_s}-1\right)}{\hat{d}_n\hat{r}_s\left(\frac{K_p}{K_s}-1\right)-\lambda_s\lambda_n} + \frac{\lambda_e\lambda_m}{\hat{r}_m\left(\frac{K_p}{K_m}-1\right)\hat{r}_e\left(\frac{K_p}{K_e}-1\right)} + \frac{f\omega_8\lambda_e}{d_h\delta_I t_{sa}\hat{r}_m\left(\frac{K_p}{K_m}-1\right)}$. By assuming that the total amount of infused cells (dose D and fraction of CCR5-editing f_p) home to the BM/Thymus rapidly, and that the amount of remaining HSPCs after TBI and immediately before transplant is $P(t_x) = P_r$, the approximate steady state for P is $\bar{P} \approx \frac{K_p}{a}\cdot\frac{(1-f_p)D+P_r}{D+P_r} = \frac{K_p}{a}\left(1-\frac{f_pD}{D+P_r}\right)$. Together this gives the following expression for the effective reproductive ratio:

$$R_{eff} = R_T\left(1-\frac{f_pD}{D+P_r}\right), \text{ with } R_T = \frac{\tau\beta\pi\lambda_e K_p}{a\gamma\delta_I\left[\frac{\hat{d}_n\hat{r}_s}{\lambda_n}\left(\frac{K_p}{K_s}-1\right)-\lambda_s\right](1+\theta\bar{E}_h)}. \quad \textbf{Equation (4)}$$

Here, R_T then represents the effective reproductive ratio during transplant in the absence of gene-editing when cells have reached steady state.

Approximate viral load set point when $r_n = 0$ and $\kappa = 0$

We calculated an approximate viral steady state after ATI assuming all derivatives in **eq. (3)** are equal to zero. This assumption leads to the equations, $\frac{\tau\beta\bar{S}\pi}{\gamma\delta_I(1+\theta\bar{E}_h)} = 1$, $\bar{S} = \frac{\lambda_f\bar{P}\left(\lambda_n+\frac{\omega_4 I_{50}\bar{I}}{\bar{I}+I_{50}}\right)}{\left(\hat{d}_n+\frac{\omega_4 I_{50}\bar{I}}{\bar{I}+I_{50}}\right)\hat{r}_s\left(\frac{K_p}{K_s}-1\right)-\lambda_s\left(\lambda_n+\frac{\omega_4 I_{50}\bar{I}}{\bar{I}+I_{50}}\right)}$, $\bar{E}_h = \frac{f\omega_8 I_{50}\frac{\beta\bar{V}\bar{S}}{\delta_I}\bar{M}}{d_h\left(\frac{\beta\bar{V}\bar{S}}{\delta_I}+I_{50}\right)}$ and $\bar{M} = \frac{\lambda_e K_p}{a\hat{r}_m\left(\frac{K_p}{K_m}-1\right)+\frac{a\omega_8(2f-1)I_{50}\bar{I}}{\bar{I}+I_{50}}}$. To obtain an approximation of the viral set point $\bar{V}$ we used the equations above and the following rules:

$$\lambda_n + \frac{\omega_4 I_{50}\bar{I}}{\bar{I}+I_{50}} \approx \begin{cases} \lambda_n, & \lambda_n \gg \omega_4 \bar{I} \\ \lambda_n + \omega_4 I_{50}, & \lambda_n < \omega_4 I_{50} \end{cases},$$

$$\hat{d}_n + \frac{\omega_4 I_{50}\bar{I}}{\bar{I}+I_{50}} \approx \begin{cases} \hat{d}_n, & \hat{d}_n \gg \omega_4 \bar{I} \\ \hat{d}_n + \omega_4 I_{50}, & \hat{d}_n < \omega_4 I_{50} \end{cases},$$

$$\hat{r}_m\left(\frac{K_p}{K_m} - 1\right) + \frac{\omega_8(2f-1)I_{50}\bar{I}}{\bar{I}+I_{50}} \approx \begin{cases} \hat{r}_m\left(\frac{K_p}{K_m} - 1\right), & \hat{r}_m\left(\frac{K_p}{K_m} - 1\right) \gg (2f-1)\omega_8 \bar{I} \\ \hat{r}_m\left(\frac{K_p}{K_m} - 1\right) + (2f-1)\omega_8 I_{50}, & \hat{r}_m\left(\frac{K_p}{K_m} - 1\right) < (2f-1)\omega_8 I_{50} \end{cases}.$$

Here, $\bar{I}$ is obtained from simulations of the model after 10 years after ATI for $I_p + I_u$ using parameter estimates from best fits to each animal data. Regardless of the assumptions above, the viral load set point is always proportional to the following term,

$$\bar{V} \propto \left(\frac{\pi d_h}{\omega_8 K_m}\right)\left(\frac{a\hat{r}_m(K_p - K_m)}{\gamma\theta f \lambda_f K_p}\right).$$

We define the ratio $\frac{\omega_8 K_m}{d_h}$ as the turnover rate of SHIV-specific CD8$^+$ T cells.

Supplementary Materials

Supplementary Methods

Supplementary Figures

Fig. S1. CD4$^+$ and CD8$^+$ T cell levels pre-ATI in control group (n = 5) at times relative to post-transplantation in WT and ΔCCR5 transplant groups.

Fig. S2. Individual fits of the best model to the blood T cell observations pre-ATI in control group from a time relative to post-transplantation in transplant groups.

Fig. S3. Individual fits of the best model to the blood T cell observations post-transplantation, pre-ATI for the wild-type-transplant group.

Fig. S4. Individual fits of the best model to the blood T cell observations post-transplantation, pre-ATI for the ΔCCR5-transplant group.

Fig. S5. Predictions of the best model for the contributors to cell expansion in $CD8^+$ T_{EM} cells in animals from the transplant groups.

Fig. S6. Correlations between viral load and $CD4^+CCR5^+$ T cells over time in each animal post-ATI.

Fig. S7. Individual fits of the best model to the blood T cell and viral load observations before/after ATI for control group.

Fig. S8. Individual fits of the best model to the blood T cell and viral load observations before/after ATI for the wild-type-transplant group.

Fig. S9. Individual fits of the best model to the blood T cell and viral load observations before/after ATI for the ΔCCR5-transplant group.

Fig. S10. Model predictions for post-rebound viral control after CCR5 gene-edited HSPC transplantation based on R_{eff}.

Fig. S11. Model predictions of the fraction of protected HSPCs in the transplant f_p (y-axis) and the fraction of transplanted HSPCs with respect to the total infused plus remaining post-TBI HSPCs $D: P_r$ (x-axis in log-scale) required for spontaneous viral control.

Supplementary Tables

Table S1. Values of the fraction of protected cells in transplant product f_p, dose or number of HSPCs in transplant product D and time of transplantation t_x of each animal for model fitting and projections.

Table S2. Competing models for fitting T cell reconstitution with respective AIC values.

Table S3. Population parameter estimates for the best fits of the model in eq. 2 in the main text (lowest AIC in Table S2) to the T cell reconstitution dynamics.

Table S4. Individual parameter estimates for the best fits of the model in eq. 2 in the main text (lowest AIC in Table S2) to the T cell reconstitution dynamics.

Table S5. Competing models for fitting T cell and viral dynamics (eqs. 2-3 in main text) using the best model in Table S2 and fixing parameter values as in Table S3, with AIC values.

Table S6. Population parameter estimates for the fits of the model with lowest AIC in Table S5 to the T cell and virus dynamics.

Table S7. Individual parameter estimates for the fits of the model in eqs. 2-3 in main text (lowest AIC in Table S5) to the T cell and virus dynamics.

Acknowledgements: Funding: This study was supported by grants from the National Institutes of Health, National Institute of Allergy and Infectious Diseases (UM1 AI126623, R01 AI150500). ERD is supported by the National Center for Advancing Translational Sciences of the National Institutes of Health under Award Number KL2 TR002317. DBR is supported by a Washington Research Foundation postdoctoral fellowship, and a CFAR NIA P30 AI027757. NHP studies were supported by NIH P51 OD010425. The funders had no role in study design, data collection and analysis, decision to publish, or preparation of the manuscript. The content is solely the responsibility of the authors and does not necessarily represent the official views of the National Institutes of Health or the Washington Research Foundation. **Author contributions:** E.F.C. and J.T.S. conceived the study. C.W.P. and H.-P.K. contributed ideas and data sources for the project. E.R.D. and D.B.R. contributed in the development of mechanistic mathematical models. B.T.M. contributed ideas and support for statistical models and analyses. E.F.C. assembled data, wrote all code, performed all calculations and derivations, ran the models, and

analyzed output data. J.T.S. and E.F.C. wrote the manuscript with contributions from all other authors. **Competing interests:** H.-P.K has served on advisory boards for Rocket Pharmaceuticals, Homology medicines and CSL for research unrelated to this manuscript. Other authors declare no competing financial interests. **Animal Welfare:** The data used in this work were collected in strict accordance with the recommendations in the *Guide for the Care and Use of Laboratory Animals* of the National Institutes of Health. The study protocol was approved by the Institutional Animal Care and Use Committees (3235-03) of the Fred Hutchinson Cancer Research Center and the University of Washington. **Data and materials availability**: Original data and code will be shared upon request.

Figures:

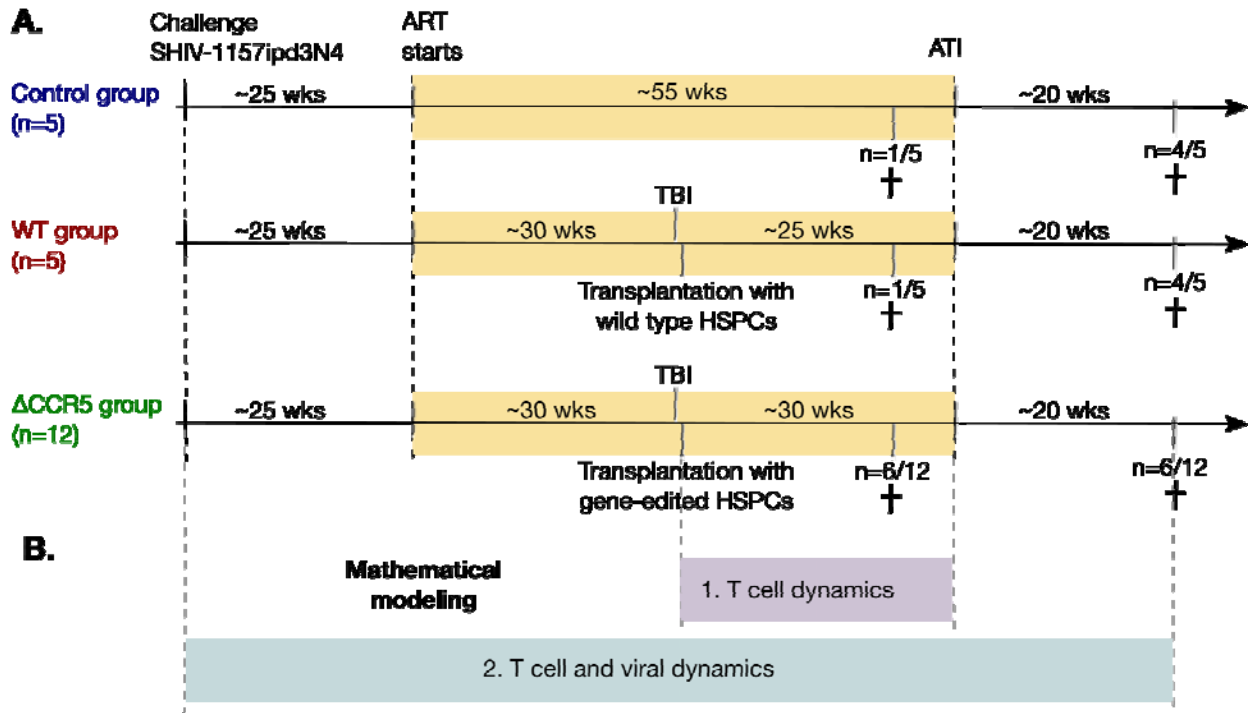

Figure 1. Study design and mathematical modeling.

A. 22 pig-tailed macaques were infected with SHIV and suppressed with ART. Next, 17/22 underwent HSPC transplantation following myeloablative conditioning (TBI), including 12 animals that received CCR5-edited products and 5 that received non-edited products (ΔCCR5 and WT groups, respectively). A control group (n=5) did not receive TBI or HSPC transplantation. Fourteen animals underwent ATI approximately one year after ART initiation, while the remaining 8 animals were necropsied prior to ATI (see Methods for details). **B.** We first developed mathematical models for T cell dynamics and reconstitution following transplant and before ATI (purple), assuming that low viral loads on ART do not affect cell dynamics. After validation of that model, we introduced viral dynamics and fit those to the T cell and viral rebound dynamics from the animals pre- and post-ATI (blue).

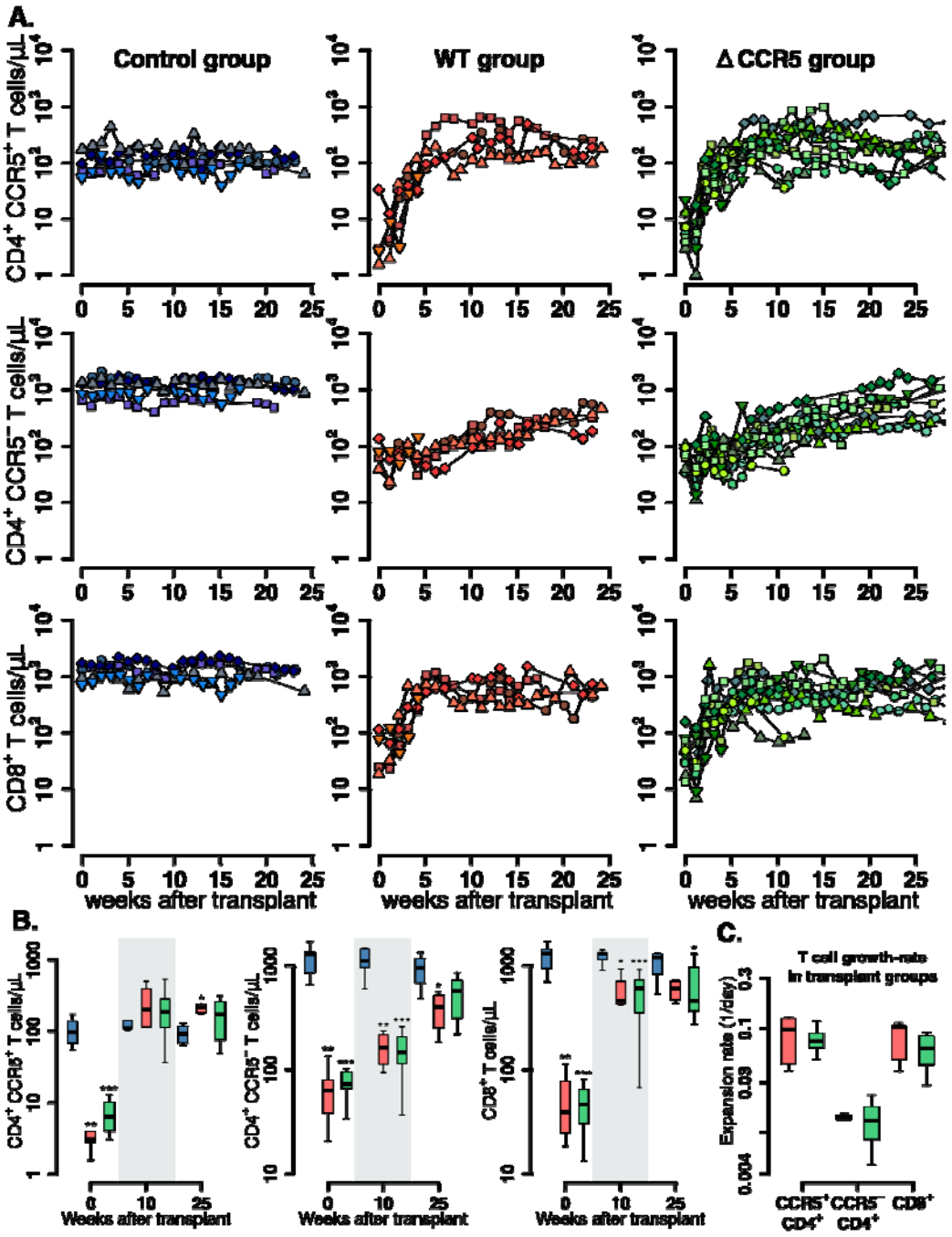

Figure 2. Post-transplantation, pre-ATI CD4$^+$ and CD8$^+$ T cell dynamics.

A. Empirical data for peripheral CD4$^+$ CCR5$^+$ (top row), CD4$^+$CCR5$^-$ (middle row) and CD8$^+$ T cell counts (bottom row) for control (blue), wild-type (red) and ΔCCR5 (green) transplantation groups. Each datapoint shape and color is a different animal sampled over time. **B.** Range of blood CD4$^+$ and CD8$^+$ T cell counts for weeks 0, 10 and 25 after transplantation (p-values

calculated with Mann-Whitney test comparing control group with transplant groups. $^{*}P<0.05$, $^{**}P<0.01$ and $^{***}P<0.001$). **C.** Expansion-rate estimates of $CD4^{+}CCR5^{+}$, $CD4^{+}CCR5^{-}$, and $CD8^{+}$ T cells (p-value calculated using a paired t-test). Colors for boxplots in **B & C** are matched to **A** **(**blue: control, red: wild-type-transplantation and green: ΔCCR5-transplantation groups).

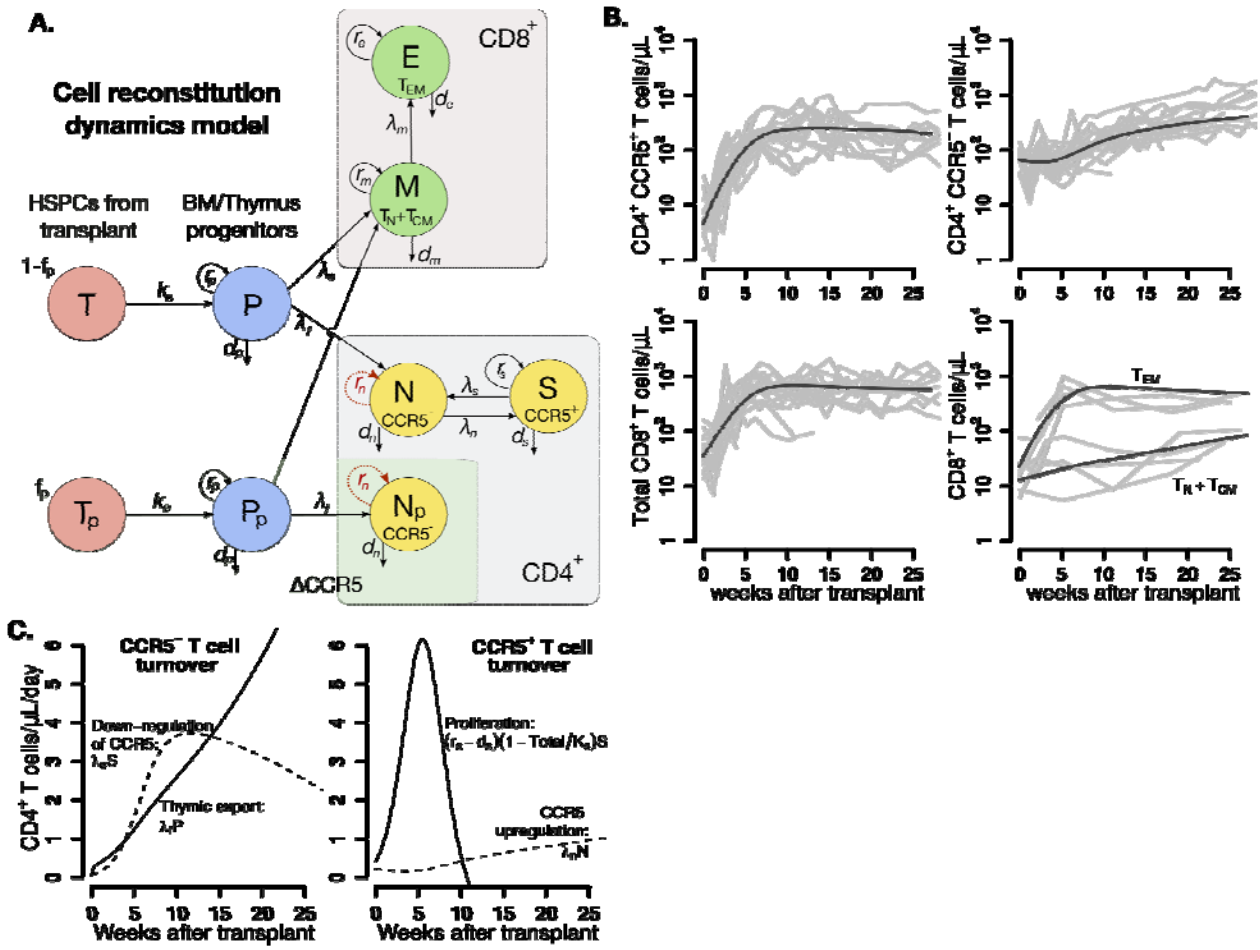

Figure 3. Mathematical model of T cell reconstitution after HSPC transplantation. **A.** Schematics of the model. Each circle represents a cell compartment: *T* represents the HSPCs from the transplant; *P*, the progenitor cells in bone marrow (BM) and thymus; *S* and *N*, $CD4^+CCR5^+$ and $CD4^+CCR5^-$ T cells, respectively; T_p, the protected (ΔCCR5), gene-modified cells from transplant; P_p, protected (ΔCCR5) progenitor cells in bone marrow/thymus; N_p the protected (ΔCCR5) $CD4^+$ T cells; *M* the $CD8^+$ T cells with naïve and central memory phenotype and *E* $CD8^+$ T cells with effector memory phenotype. The initial fraction of protected cells is represented by the parameter f_p. Gray panels represent mature blood $CD4^+$ and $CD8^+$ T cells, and green panel all ΔCCR5 cells in the model. Red, dashed arrows represent discarded terms after model selection and validation (see text for details). **B.** Model predictions using the maximum

likelihood estimation of the population parameters (solid black lines) for all blood T cell subsets before ATI for all animals in the transplant groups. Each gray line is one animal. **C.** Model predictions of the total concentration of $CD4^{+}CCR5^{-}$ T cells generated by CCR5 downregulation (dashed line) or thymic export (solid line), and of the total concentration of $CD4^{+}CCR5^{+}$ T cells generated by proliferation (solid line) or by up-regulation of CCR5 (dashed line) over time using the maximum likelihood estimation of the population parameters.

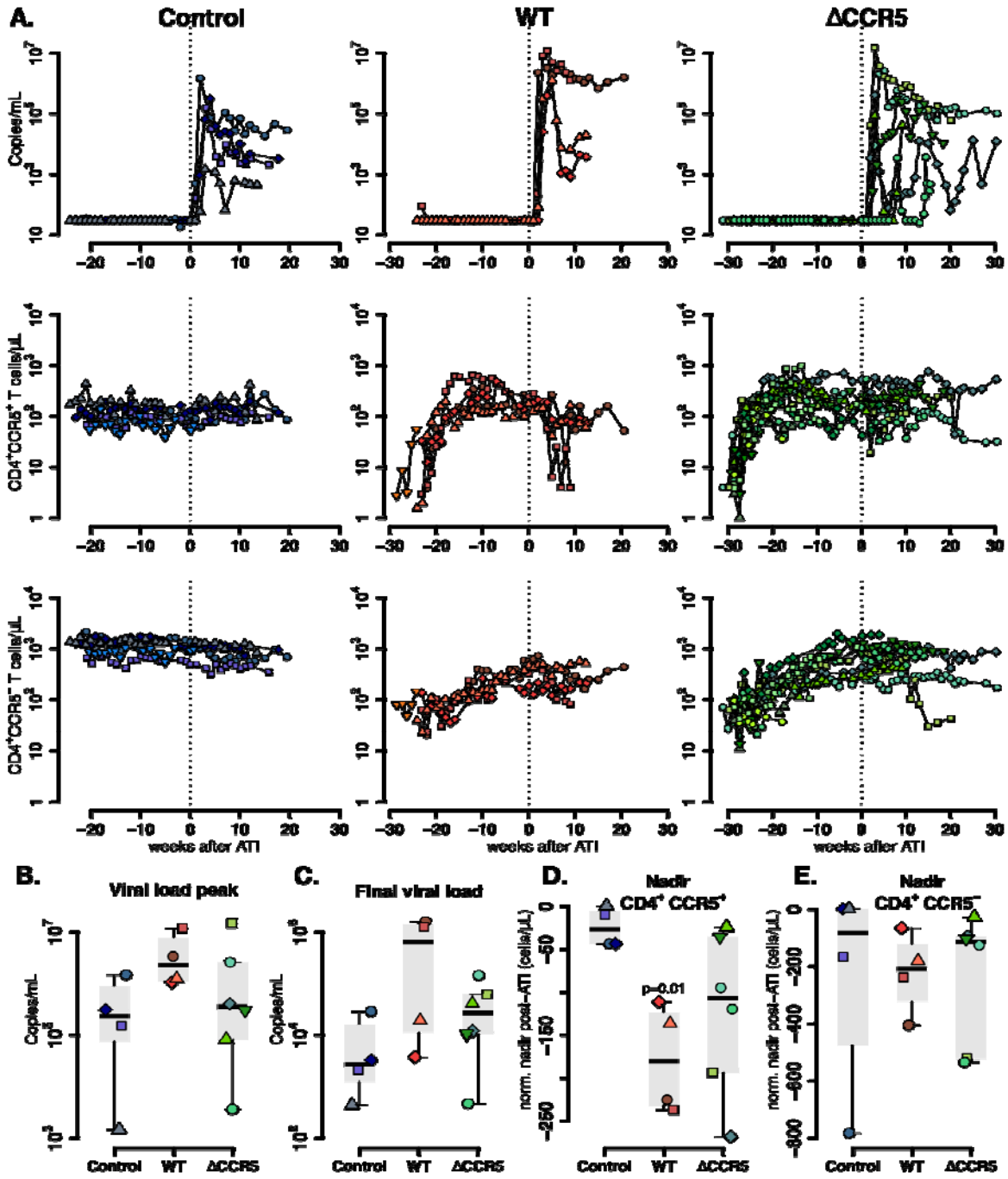

Figure 4. Plasma viral load and CD4$^+$ T cell kinetics after ATI.

A. Empirical data for viral load (top row) and peripheral T cell counts (middle and bottom rows) for control (blue), wild-type (red) and ΔCCR5 (green) transplantation groups. Each datapoint shape and color is a different animal sampled over time. **B-E**: Distributions of **B.** peak viral load post-ATI, **C.** viral load at endpoint necropsy, **D.** CD4$^+$CCR5$^+$ T-cell nadir post-ATI normalized

relative to the $CD4^+CCR5^+$ concentration at ATI, **E.** $CD4^+CCR5^-$ T-cell nadir post-ATI normalized relative to the $CD4^+CCR5^-$ concentration at ATI. Controls were compared to transplant groups using Mann-Whitney test for all summary measures.

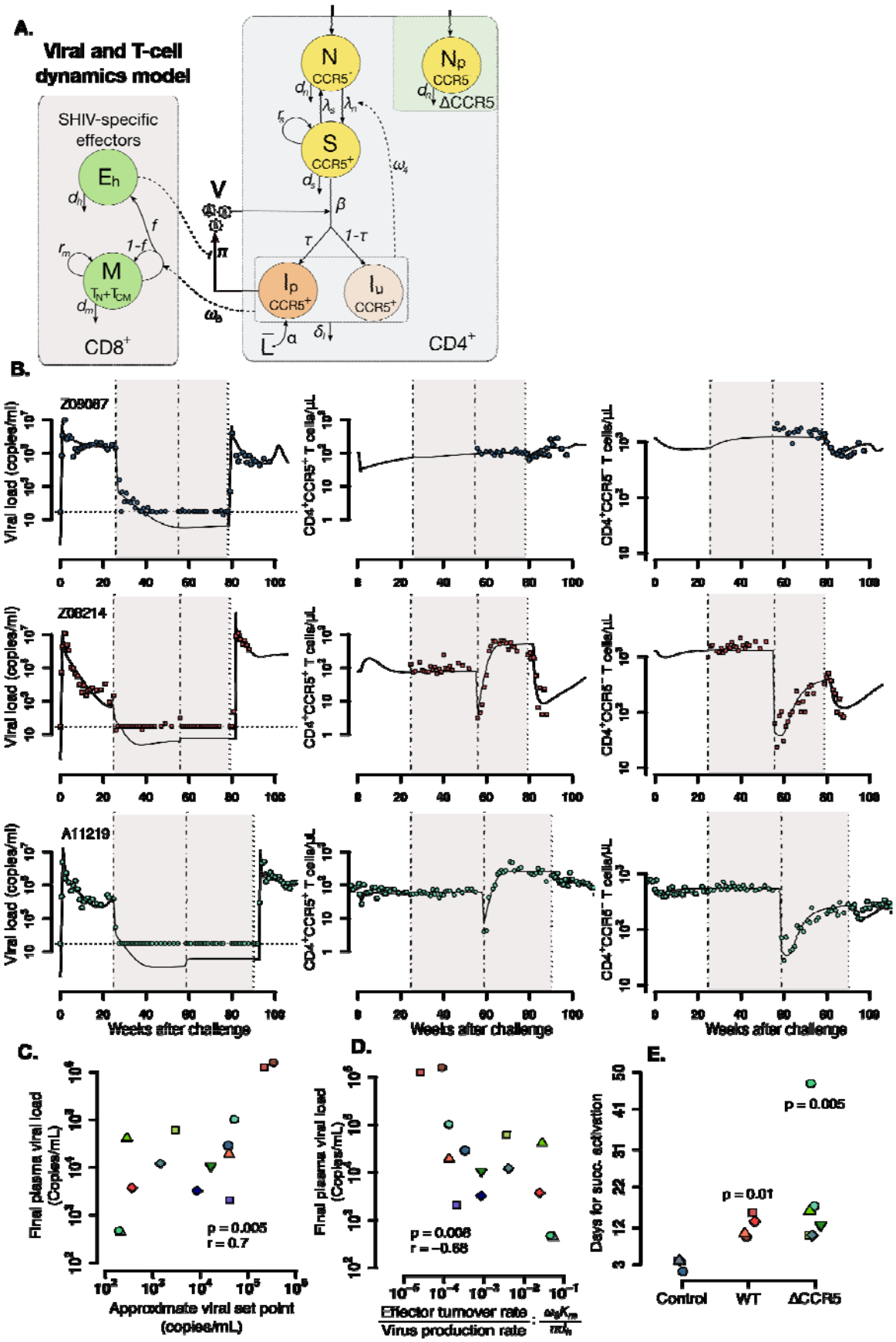
A.
Viral and T-cell dynamics model
SHIV-specific effectors
CD8+
CD4+
ΔCCR5
B.
Z09087
Z08214
A11219
Viral load (copies/ml)
Weeks after challenge
C.
Final plasma viral load (Copies/mL)
Approximate viral set point (copies/mL)
p = 0.005
r = 0.7
D.
p = 0.008
r = −0.68
Effector turnover rate / Virus production rate
E.
Days for succ. activation
p = 0.005
p = 0.01
Control
WT
ΔCCR5

644

Figure 5. Mathematical model of virus and T cell dynamics following ATI.

A. Model: Susceptible cells, S, are infected by the virus, V, at rate β. I_p represents the fraction τ of the infected cells that produce virus, and, I_u, the other fraction that becomes unproductively infected. Total $CD4^+CCR5^+$ T cell count is given by the sum of S, I_p and I_u. All infected cells die at rate δ_I. I_P cells arise from activation of latently infected cells at rate $\alpha\bar{L}$ and produce at a rate π virus that is cleared at rate γ. $CD8^+$ M cells proliferate in the presence of infection with rate ω_8 from which a fraction f become SHIV-specific $CD8^+$ effector T cells, E_h, that are removed at a rate d_h. These effector cells reduce virus production (π) by $1/(1+\theta E_h)$. Non-susceptible $CD4^+$ T cells that were not CCR5-edited upregulate CCR5 in the presence of infection and replenish the susceptible pool at rate ω_4. Gray panels represent mature blood $CD4^+$ and $CD8^+$ T cells, and green panel ΔCCR5 cells in the model. **B.** Individual fits of the model (black lines) to SHIV RNA (left column), blood $CD4^+CCR5^+$ T cells (middle column) and $CD4^+CCR5^-$ T cells (right column) for one animal in the control (top row), wild type (middle row) and ΔCCR5 groups (bottom row). Shaded areas represent time during ART and dashed-point line, the time of transplantation. **C-D:** Scatterplots of final observed viral load vs. **C.** Approximate viral set points obtained by the model, and **D.** the ratio between the turnover rate of SHIV-specific $CD8^+$ T cells and the virus production rate: $\frac{\left(\frac{\omega_8 K_m}{d_h}\right)}{\pi}$ (p-values calculated using Pearson's correlation test). **E.** Individual estimates of the time until SHIV successful activation after ATI (see **Methods**). Blue: control, red: wild type, and green: ΔCCR5 transplant group (p-values calculated by Mann-Whitney test).

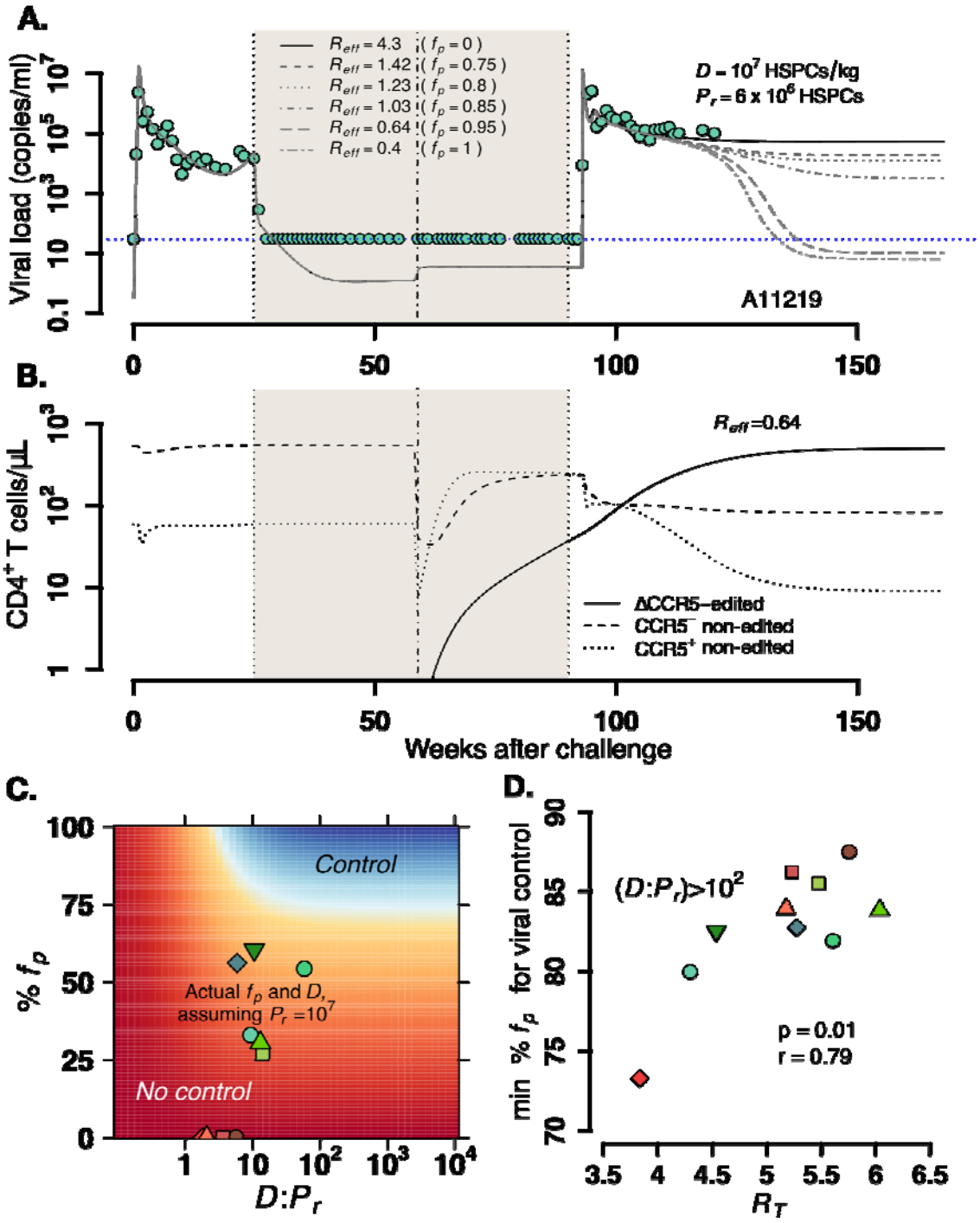

Figure 6. Model predictions of factors governing post-rebound viral control after CCR5 gene-edited HSPC transplant.

A. Predictions for plasma viral loads post-ATI using the optimized mathematical model. Here,

—— and is the composite determinant of viral control. Parameter estimates for

animal A11219 (**Table S7)** were used to compute the effective reproductive ratio R_T . Higher values of R_T imply poorer anti-SHIV immunity (see **eq. 4** in Methods). We varied values of the fraction of HSPCs in transplant f_p, the stem cell dose D as shown and fixed the remaining number of HSPCs after TBI before transplant $P_r = 6 \times 10^6$. $R_{eff} < 1$ predicted spontaneous viral control 40-50 weeks after ATI. **B.** A simulation with $R_{eff} = 0.64$ demonstrates CCR5-edited CD4+ T cell recovery is concurrent with viral control. **C.** Model predictions of the fraction of protected HSPCs in the transplant f_p (y-axis) and the fraction of transplanted HSPCs with respect to the total infused plus remaining post-TBI HSPCs $D{:}P_r$ (x-axis) required for spontaneous viral control. $R_T = 3.7$ is from animal A11200 which has the lowest f_p (74%) and $D{:}P_r$ (~10) required for post-ATI viral control (heatmaps for other animals in **Fig. S11**). Blue color represents the parameter space with post-ATI viral control or $R_{eff} < 1$. Yellow-to-red colors represent the parameter space with no control or $R_{eff} > 1$. Data points represent the individual values of f_p and $D{:}P_r$ from each transplanted animal in the study. **D.** Model predictions of the minimum fraction of protected HSPCs in the body f_p for viral control (y-axis) when $\frac{D}{P_r} > 100$ is assumed for each animal given their calculated values for R_T (x-axis). Each color is an animal, and A11200 is the red diamond with the lowest value of min f_p. A lower f_p may lead to viral control if there is a more potent anti-SHIV immune response.

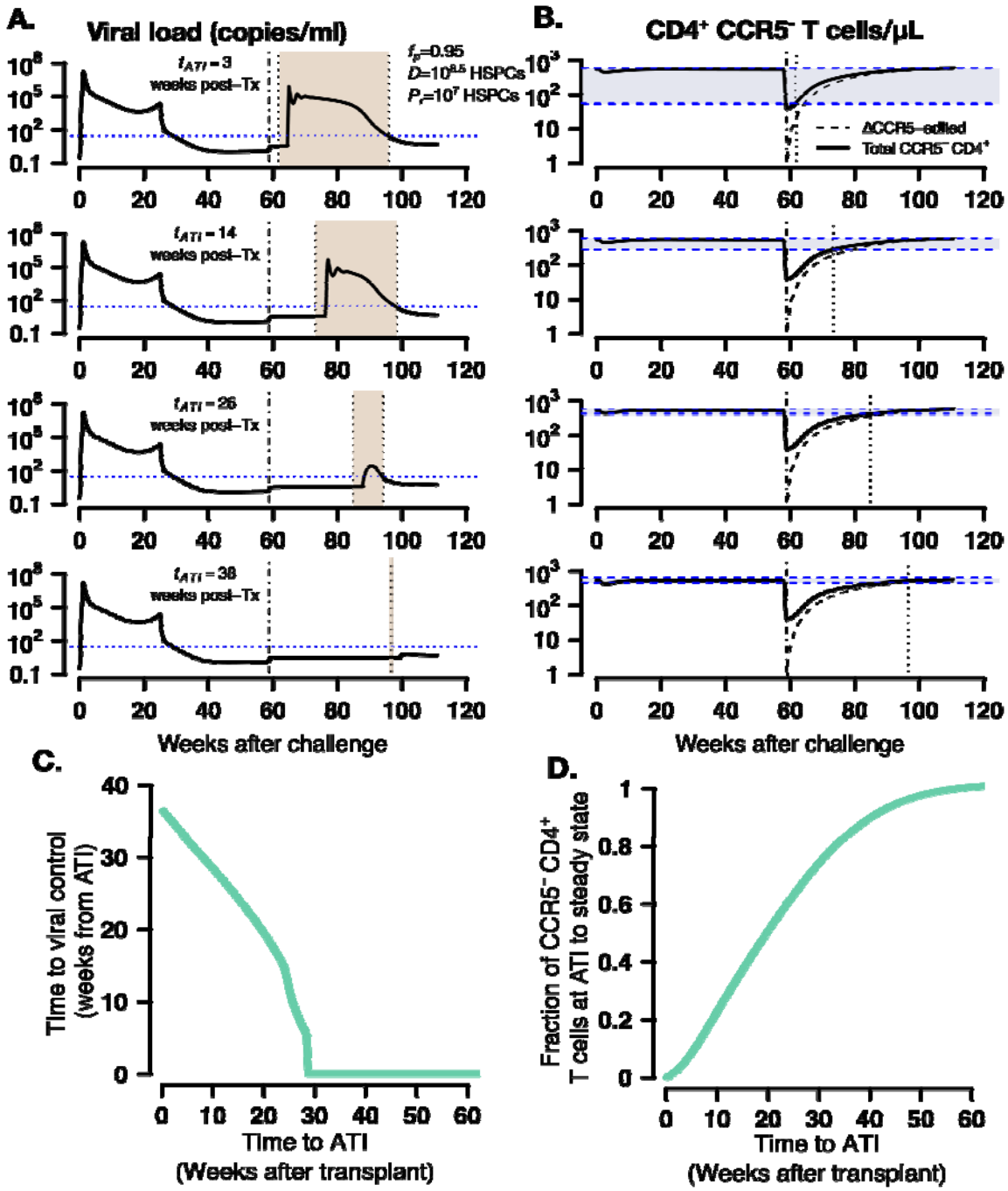

Figure 7. Model predictions of time to post-ATI viral control given varying times for the start of ATI.

A-B. Examples of projected **A.** viral load and **B.** total $CD4^+$ $CCR5^-$ and ΔCCR5 $CD4^+$ T cells from the model for animal A11219 when , HSPCs and HSPCs, for different times of ATI (= 3, 14, 26 and 38 weeks after transplantation). Dashed-dotted

vertical lines represent time of transplant. Shaded areas between the dotted lines in **A.** describe the time from ATI until spontaneous viral control. Shaded areas between the blue dashed lines in **B.** represent the difference between the $CD4^+$ $CCR5^-$ T cell concentration at ATI and the projected steady state. Dotted lines in **B.** represent time of ATI. **C-D.** Model predictions of the **C.** time until viral control after ATI and **D.** the fraction of total $CD4^+$ $CCR5^-$ T cell concentration at ATI with respect to its steady state for varying times of ATI between 0 and 60 weeks after transplant for animal A11219.

References

1. T.-W. Chun *et al.*, Quantification of latent tissue reservoirs and total body viral load in HIV-1 infection. *Nature* **387**, 183 (1997).
2. T.-W. Chun *et al.*, In vivo fate of HIV-1-infected T cells: Quantitative analysis of the transition to stable latency. *Nature Medicine* **1**, 1284-1290 (1995).
3. D. Finzi *et al.*, Identification of a Reservoir for HIV-1 in Patients on Highly Active Antiretroviral Therapy. *Science* **278**, 1295-1300 (1997).
4. K. Allers *et al.*, Evidence for the cure of HIV infection by CCR5Δ32/Δ32 stem cell transplantation. *Blood* **117**, 2791-2799 (2011).
5. G. Hütter *et al.*, Long-Term Control of HIV by CCR5 Delta32/Delta32 Stem-Cell Transplantation. *New England Journal of Medicine* **360**, 692-698 (2009).
6. R. K. Gupta *et al.*, HIV-1 remission following CCR5Δ32/Δ32 haematopoietic stem-cell transplantation. *Nature*, 1 (2019).
7. T. J. Henrich *et al.*, CCR5-Δ32 Heterozygosity, HIV-1 Reservoir Size, and Lymphocyte Activation in Individuals Receiving Long-term Suppressive Antiretroviral Therapy. *The Journal of Infectious Diseases* **213**, 766-770 (2016).
8. T. J. Henrich *et al.*, Antiretroviral-Free HIV-1 Remission and Viral Rebound After Allogeneic Stem Cell Transplantation: Report of 2 Cases. *Annals of Internal Medicine* **161**, 319 (2014).
9. T. J. Henrich *et al.*, Long-Term Reduction in Peripheral Blood HIV Type 1 Reservoirs Following Reduced-Intensity Conditioning Allogeneic Stem Cell Transplantation. *The Journal of Infectious Diseases* **207**, 1694-1702 (2013).
10. M. Salgado *et al.*, Mechanisms That Contribute to a Profound Reduction of the HIV-1 Reservoir After Allogeneic Stem Cell Transplant. *Annals of Internal Medicine*, (2018).
11. P. Tebas *et al.*, Gene Editing of CCR5 in Autologous CD4 T Cells of Persons Infected with HIV. *New England Journal of Medicine* **370**, 901-910 (2014).
12. C. W. Peterson *et al.*, Long-term multilineage engraftment of autologous genome-edited hematopoietic stem cells in nonhuman primates. *Blood* **127**, 2416-2426 (2016).
13. C. W. Peterson *et al.*, Loss of immune homeostasis dictates SHIV rebound after stem-cell transplantation. *JCI Insight* **2**, (2017).
14. C. W. Peterson *et al.*, Differential impact of transplantation on peripheral and tissue-associated viral reservoirs: Implications for HIV gene therapy. *PLOS Pathogens* **14**, e1006956 (2018).
15. S. C. Jameson, Maintaining the norm: T-cell homeostasis. *Nature Reviews Immunology* **2**, 547-556 (2002).
16. K. S. Schluns, K. Williams, A. Ma, X. X. Zheng, L. Lefrançois, Cutting Edge: Requirement for IL-15 in the Generation of Primary and Memory Antigen-Specific CD8 T Cells. *The Journal of Immunology* **168**, 4827-4831 (2002).
17. K. S. Schluns, W. C. Kieper, S. C. Jameson, L. Lefrançois, Interleukin-7 mediates the homeostasis of naïve and memory CD8 T cells *in vivo*. *Nature Immunology* **1**, 426-432 (2000).
18. A. W. Goldrath, C. J. Luckey, R. Park, C. Benoist, D. Mathis, The molecular program induced in T cells undergoing homeostatic proliferation. *Proceedings of the National Academy of Sciences* **101**, 16885-16890 (2004).

19. D. Voehringer, H.-E. Liang, R. M. Locksley, Homeostasis and Effector Function of Lymphopenia-Induced “Memory-Like” T Cells in Constitutively T Cell-Depleted Mice. *The Journal of Immunology* **180**, 4742-4753 (2008).
20. D. C. Douek *et al.*, Assessment of thymic output in adults after haematopoietic stemcell transplantation and prediction of T-cell reconstitution. *The Lancet* **355**, 1875-1881 (2000).
21. D. C. Douek *et al.*, Changes in thymic function with age and during the treatment of HIV infection. *Nature* **396**, 690-695 (1998).
22. J. Bender, T. Mitchell, J. Kappler, P. Marrack, Cd4+ T Cell Division in Irradiated Mice Requires Peptides Distinct from Those Responsible for Thymic Selection. *Journal of Experimental Medicine* **190**, 367-374 (1999).
23. W. C. Kieper, S. C. Jameson, Homeostatic expansion and phenotypic conversion of naïve T cells in response to self peptide/MHC ligands. *Proceedings of the National Academy of Sciences* **96**, 13306-13311 (1999).
24. F. Sallusto, J. Geginat, A. Lanzavecchia, Central Memory and Effector Memory T Cell Subsets: Function, Generation, and Maintenance. *Annual Review of Immunology* **22**, 745-763 (2004).
25. C. L. Saout, S. Mennechet, N. Taylor, J. Hernandez, Memory-like CD8+ and CD4+ T cells cooperate to break peripheral tolerance under lymphopenic conditions. *Proceedings of the National Academy of Sciences* **105**, 19414-19419 (2008).
26. J. Sprent, C. D. Surh, Normal T cell homeostasis: the conversion of naive cells into memory-phenotype cells. *Nature Immunology* **12**, 478-484 (2011).
27. D. B. Reeves, C. W. Peterson, H.-P. Kiem, J. T. Schiffer, Autologous Stem Cell Transplantation Disrupts Adaptive Immune Responses during Rebound Simian/Human Immunodeficiency Virus Viremia. *Journal of Virology* **91**, e00095-00017 (2017).
28. M. Elemans *et al.*, Why Don't CD8+ T Cells Reduce the Lifespan of SIV-Infected Cells In Vivo? *PLOS Computational Biology* **7**, e1002200 (2011).
29. N. R. Klatt *et al.*, CD8+ Lymphocytes Control Viral Replication in SIVmac239-Infected Rhesus Macaques without Decreasing the Lifespan of Productively Infected Cells. *PLOS Pathogens* **6**, e1000747 (2010).
30. J. K. Wong *et al.*, In Vivo CD8+ T-Cell Suppression of SIV Viremia Is Not Mediated by CTL Clearance of Productively Infected Cells. *PLOS Pathogens* **6**, e1000748 (2010).
31. V. Shridhar, Y. Chen, P. Gupta, The CD8 Antiviral Factor (CAF) can suppress HIV-1 transcription from the Long Terminal Repeat (LTR) promoter in the absence of elements upstream of the CATATAA box. *Virology Journal* **11**, 130 (2014).
32. D. Blazek, F. Teque, C. Mackewicz, M. Peterlin, J. A. Levy, The CD8+ cell non-cytotoxic antiviral response affects RNA polymerase II-mediated human immunodeficiency virus transcription in infected CD4+ cells. *Journal of General Virology* **97**, 220-224 (2016).
33. L. Zhang *et al.*, Contribution of Human α-Defensin 1, 2, and 3 to the Anti-HIV-1 Activity of CD8 Antiviral Factor. *Science* **298**, 995-1000 (2002).
34. D. C. Douek, L. J. Picker, R. A. Koup, T Cell Dynamics in HIV-1 Infection. *Annual Review of Immunology* **21**, 265-304 (2003).
35. A. Okoye *et al.*, Progressive CD4+ central–memory T cell decline results in CD4+ effector–memory insufficiency and overt disease in chronic SIV infection. *Journal of Experimental Medicine* **204**, 2171-2185 (2007).

36. A. A. Okoye *et al.*, Naive T cells are dispensable for memory CD4+ T cell homeostasis in progressive simian immunodeficiency virus infection. *Journal of Experimental Medicine* **209**, 641-651 (2012).
37. K. P. Burnham, D. R. Anderson, *Model Selection and Multimodel Inference: A Practical Information-Theoretic Approach*. (Springer-Verlag, New York, ed. 2, 2002).
38. K. G. Haworth, C. W. Peterson, H.-P. Kiem, CCR5-edited gene therapies for HIV cure: Closing the door to viral entry. *Cytotherapy* **19**, 1325-1338 (2017).
39. A. Zhen *et al.*, Long-term persistence and function of hematopoietic stem cell-derived chimeric antigen receptor T cells in a nonhuman primate model of HIV/AIDS. *PLOS Pathogens* **13**, e1006753 (2017).
40. T. Guillaume, D. B. Rubinstein, M. Symann, Immune Reconstitution and Immunotherapy After Autologous Hematopoietic Stem Cell Transplantation. *Blood* **92**, 1471-1490 (1998).
41. W. Krenger, B. R. Blazar, G. A. Holländer, Thymic T-cell development in allogeneic stem cell transplantation. *Blood* **117**, 6768-6776 (2011).
42. E. Roux *et al.*, Recovery of immune reactivity after T-cell–depleted bone marrow transplantation depends on thymic activity. *Blood* **96**, 2299-2303 (2000).
43. R. E. Donahue *et al.*, Discordance in lymphoid tissue recovery following stem cell transplantation in rhesus macaques: an in vivo imaging study. *Blood* **126**, 2632-2641 (2015).
44. S. Radtke *et al.*, A distinct hematopoietic stem cell population for rapid multilineage engraftment in nonhuman primates. *Science Translational Medicine* **9**, eaan1145 (2017).
45. R. Mehr, A. S. Perelson, Blind T-cell homeostasis and the CD4/CD8 ratio in the thymus and peripheral blood. *Journal of Acquired Immune Deficiency Syndromes and Human Retrovirology: Official Publication of the International Retrovirology Association* **14**, 387-398 (1997).
46. J. B. Margolick, A. D. Donnenberg, T-cell homeostasis in HIV-1 infection. *Seminars in Immunology* **9**, 381-388 (1997).
47. H. Spits, Development of αβ T cells in the human thymus. *Nature Reviews Immunology* **2**, 760 (2002).
48. V. R. Buchholz *et al.*, Disparate Individual Fates Compose Robust CD8+ T Cell Immunity. *Science* **340**, 630-635 (2013).
49. D. L. Farber, N. A. Yudanin, N. P. Restifo, Human memory T cells: generation, compartmentalization and homeostasis. *Nature Reviews Immunology* **14**, 24-35 (2014).
50. S. M. Kaech, E. J. Wherry, R. Ahmed, Effector and memory T-cell differentiation: implications for vaccine development. *Nature Reviews Immunology* **2**, 251-262 (2002).
51. C. Tanchot, F. A. Lemonnier, B. Pérarnau, A. A. Freitas, B. Rocha, Differential Requirements for Survival and Proliferation of CD8 Naïve or Memory T Cells. *Science* **276**, 2057-2062 (1997).
52. J. T. Tan *et al.*, IL-7 is critical for homeostatic proliferation and survival of naïve T cells. *Proceedings of the National Academy of Sciences* **98**, 8732-8737 (2001).
53. T. Stiehl, A. Marciniak-Czochra, Characterization of stem cells using mathematical models of multistage cell lineages. *Mathematical and Computer Modelling* **53**, 1505-1517 (2011).
54. T. Stiehl, N. Baran, A. D. Ho, A. Marciniak-Czochra, Clonal selection and therapy resistance in acute leukaemias: mathematical modelling explains different proliferation

patterns at diagnosis and relapse. *Journal of The Royal Society Interface* **11**, 20140079 (2014).

55. T. Stiehl, A. Marciniak-Czochra, Stem cell self-renewal in regeneration and cancer: Insights from mathematical modeling. *Current Opinion in Systems Biology* **5**, 112-120 (2017).

56. C. C. Bleul, L. Wu, J. A. Hoxie, T. A. Springer, C. R. Mackay, The HIV coreceptors CXCR4 and CCR5 are differentially expressed and regulated on human T lymphocytes. *Proceedings of the National Academy of Sciences* **94**, 1925-1930 (1997).

57. M. B. Zaitseva *et al.*, CXCR4 and CCR5 on Human Thymocytes: Biological Function and Role in HIV-1 Infection. *The Journal of Immunology* **161**, 3103-3113 (1998).

58. R. D. Berkowitz, K. P. Beckerman, T. J. Schall, J. M. McCune, CXCR4 and CCR5 Expression Delineates Targets for HIV-1 Disruption of T Cell Differentiation. *The Journal of Immunology* **161**, 3702-3710 (1998).

59. J. M. McCune, Thymic function in HIV-1 disease. *Seminars in Immunology* **9**, 397-404 (1997).

60. A. S. Perelson, Modelling viral and immune system dynamics. *Nature Reviews Immunology* **2**, 28-36 (2002).

61. A. S. Perelson *et al.*, Decay characteristics of HIV-1-infected compartments during combination therapy. *Nature* **387**, 188 (1997).

62. A. L. Hill, D. I. S. Rosenbloom, M. A. Nowak, R. F. Siliciano, Insight into treatment of HIV infection from viral dynamics models. *Immunological Reviews* **285**, 9-25 (2018).

63. E. N. Borducchi *et al.*, Ad26/MVA therapeutic vaccination with TLR7 stimulation in SIV-infected rhesus monkeys. *Nature* **540**, 284 (2016).

64. R. J. De Boer, Understanding the Failure of CD8+ T-Cell Vaccination against Simian/Human Immunodeficiency Virus. *Journal of Virology* **81**, 2838-2848 (2007).

65. D. Wodarz, M. A. Nowak, Specific therapy regimes could lead to long-term immunological control of HIV. *Proceedings of the National Academy of Sciences* **96**, 14464-14469 (1999).

66. A. Pandit, R. J. d. Boer, HIV-1 CCR5 gene therapy will fail unless it is combined with a suicide gene. *Scientific Reports* **5**, srep18088 (2015).

67. O. Ho *et al.*, Pathogenic infection of Macaca nemestrinawith a CCR5-tropic subtype-C simian-human immunodeficiency virus. *Retrovirology* **6**, 65 (2009).

68. G. Doitsh *et al.*, Abortive HIV Infection Mediates CD4 T Cell Depletion and Inflammation in Human Lymphoid Tissue. *Cell* **143**, 789-801 (2010).

69. L. Matrajt, P. M. Younan, H.-P. Kiem, J. T. Schiffer, The Majority of CD4+ T-Cell Depletion during Acute Simian-Human Immunodeficiency Virus SHIV89.6P Infection Occurs in Uninfected Cells. *Journal of Virology* **88**, 3202-3212 (2014).

70. J. M. Conway, A. S. Perelson, J. Z. Li, Predictions of time to HIV viral rebound following ART suspension that incorporate personal biomarkers. *PLOS Computational Biology* **15**, e1007229 (2019).

71. A. L. Hill, D. I. S. Rosenbloom, F. Fu, M. A. Nowak, R. F. Siliciano, Predicting the outcomes of treatment to eradicate the latent reservoir for HIV-1. *Proceedings of the National Academy of Sciences* **111**, 13475-13480 (2014).

72. M. Prague *et al.*, Viral rebound kinetics following single and combination immunotherapy for HIV/SIV. *bioRxiv*, (2019).

73. M. A. J. *et al.*, A new theory of cytotoxic T–lymphocyte memory: implications for HIV treatment. *Philosophical Transactions of the Royal Society of London. Series B: Biological Sciences* **355**, 329-343 (2000).
74. E. F. Cardozo, C. Apetrei, I. Pandrea, R. M. Ribeiro, The dynamics of simian immunodeficiency virus after depletion of CD8+ cells. *Immunological Reviews* **285**, 26-37 (2018).
75. O. A. A., P. L. J., CD4+ T□cell depletion in HIV infection: mechanisms of immunological failure. *Immunological Reviews* **254**, 54-64 (2013).
76. M. Lavielle, *Mixed Effects Models for the Population Approach: Models, Tasks, Methods and Tools.* (Chapman and Hall/CRC, Boca Raton, ed. 1 edition, 2014), pp. 383.
77. T. Lapidot, A. Dar, O. Kollet, How do stem cells find their way home? *Blood* **106**, 1901-1910 (2005).
78. J. Chute, Stem cell homing. *Current Opinion in Hematology* **13**, 399-406 (2006).
79. B. Ramratnam *et al.*, Rapid production and clearance of HIV-1 and hepatitis C virus assessed by large volume plasma apheresis. *The Lancet* **354**, 1782-1785 (1999).
80. M. Markowitz *et al.*, A Novel Antiviral Intervention Results in More Accurate Assessment of Human Immunodeficiency Virus Type 1 Replication Dynamics and T-Cell Decay In Vivo. *Journal of Virology* **77**, 5037-5038 (2003).
81. E. F. Cardozo *et al.*, Treatment with integrase inhibitor suggests a new interpretation of HIV RNA decay curves that reveals a subset of cells with slow integration. *PLOS Pathogens* **13**, e1006478 (2017).